Spontaneous exchange of leader-laggard relationship in mutually coupled synchronized semiconductor lasers

Kazutaka Kanno,[1,*] Takuya Hida,[2] Atsushi Uchida,[2,†] and Masatoshi Bunsen[1,‡]

[1]*Department of Electronics Engineering and Computer Science, Fukuoka University, 8-19-1 Nanakuma, Johnan-ku, Fukuoka 814-0180, Japan*

[2]*Department of Information and Computer Sciences, Saitama University, 255 Shimo-okubo, Sakura-ku, Saitama City, Saitama 338-8570, Japan*

(Received 23 January 2017; published 17 May 2017)

We investigate the instantaneous behavior of synchronized temporal wave forms in two mutually coupled semiconductor lasers numerically and experimentally. The temporal wave forms of two lasers are synchronized with a propagation delay time, with one laser oscillating in advance of the other, known as the leader-laggard relationship. The leader-laggard relationship can be determined by measuring the cross-correlation between the two temporal wave forms with the propagation delay time. The leader can be identified when the optical carrier frequency of the leader laser is higher than that of the other laser. However, spontaneous exchange between the leader and laggard lasers can be observed in low-frequency fluctuations by short-term cross-correlation measurements, even for a fixed initial optical frequency detuning. The spontaneous exchange of the leader-laggard relationship originates from alternation of partial optical frequency locking between the two lasers. This observation is analyzed using a phase space trajectory on steady-state solutions for mutually coupled lasers with optical frequency detuning.

DOI: 10.1103/PhysRevE.95.052212

I. INTRODUCTION

Coupled nonlinear dynamical systems show various synchronization phenomena in chaotic dynamics, such as identical synchronization [1–3], generalized synchronization [4–6], and phase synchronization [7–9]. Synchronization of chaotic dynamics is crucial in numerous interdisciplinary research fields, such as information exchange and the binding problem in the brain [10,11], secure communications [12], and secure key exchange [13–15]. Coupled semiconductor lasers have been used as test-beds for observing a variety of synchronization phenomena [16–20].

In coupled lasers, one of two lasers oscillates in advance of the other by a propagation delay time. This phenomenon is called the leader-laggard relationship [17], a type of lag synchronization [21–23] for which two temporal wave forms are synchronized with a propagation delay time. The laser oscillating in advance is called the "leader" and the other laser is called the "laggard." Leader-laggard synchronization has been investigated in mutually coupled semiconductor lasers [24–27] and vertical-cavity surface-emitting lasers [28]. The leader and laggard lasers can be identified from the intensity dropouts of the two lasers, which occur earlier in the leader laser than in the laggard laser in the low-frequency fluctuation (LFF) regime, where LFFs are characterized by sudden dropouts at irregular times and a gradual recovery in the optical outputs [29–33]. The leader-laggard relationship can be determined only at the timing of the intensity dropouts of the LFFs. It is currently not well understood how the leader-laggard relationship changes for the short-term duration corresponding to the propagation delay time. In addition, the leader-laggard relationship in other dynamical regimes (e.g., coherence collapse) has not yet been well investigated.

A typical feature of LFF is a sudden power dropout with a following gradual power recovery. The power dropout and the recovery process in LFF are irregular, and they are associated with fast chaotic pulsations. It is known that LFF dynamics can be interpreted as chaotic itinerancy, since the laser output power hops around external-cavity modes due to saddle-node instability [29–33]. Chaotic itinerancy is a universal dynamics in high-dimensional dynamical systems, showing itinerant motion and irregular switching among different quasiattractors [34–37]. Chaotic itinerancy has been investigated in coupled systems [38,39] and networks [40], and chaotic itinerancy is considered to be important for memory searching processes [34,41] and information processing [34,42] in the human brain. Synchronization with the leader-laggard relationship can be observed in neural networks, and it is important to understand the roles played by synchronization and chaotic itinerancy in information processing in the human brain. The leader-laggard relationship for a short-term duration may reveal important information for understanding the mechanism of synchronization in delay-coupled dynamical systems.

In this study, we investigate spontaneous exchange of the leader-laggard relationship in mutually coupled semiconductor lasers in the LFF regime. We use the cross-correlation of the temporal wave forms of the mutually coupled lasers to identify the leader-laggard relationship. We then numerically investigate both the global and local leader-laggard relationship by changing the length of the temporal wave forms used for calculating the cross-correlation. We analyze steady-state solutions of the mutually coupled semiconductor lasers and explain how the local leader-laggard relationship emerges in the phase space. We also confirm the spontaneous exchange of the leader-laggard relationship in experiment.

*kkanno@fukuoka-u.ac.jp
†auchida@mail.saitama-u.ac.jp
‡bunsen@fukuoka-u.ac.jp

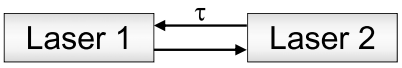

FIG. 1. Model for mutually coupled semiconductor lasers with time delay. τ is the propagation delay time of the light.

II. NUMERICAL SIMULATION

A. Numerical model

The model for mutually coupled semiconductor lasers used in our study is shown in Fig. 1. The optical output from laser 1 is injected into laser 2 after the propagation delay time τ. The optical output from laser 2 is also injected into laser 1. The coupled lasers are mathematically treated as infinite-dimensional systems due to the existence of time-delayed coupling [43]. A variety of dynamics have been observed in mutually coupled lasers, such as localized synchronization [44] and synchronized chaotic dynamics with spontaneous symmetry breaking [17,24].

The nonlinear dynamics of coupled lasers are described by the Lang-Kobayashi equations [45]:

$$\frac{dE_{1,2}(t)}{dt} = \frac{1+i\alpha}{2}\left[\frac{G_N[N_{1,2}(t)-N_0]}{1+\varepsilon|E_{1,2}(t)|^2} - \frac{1}{\tau_p}\right]E_{1,2}(t), + \kappa E_{2,1}(t-\tau)\exp[i\theta_{1,2}(t)] \quad (1)$$

$$\frac{dN_{1,2}(t)}{dt} = J - \frac{N_{1,2}(t)}{\tau_s} - \frac{G_N[N_{1,2}(t)-N_0]}{1+\varepsilon|E_{1,2}(t)|^2}|E_{1,2}(t)|^2, \quad (2)$$

$$\theta_{1,2}(t) = (\omega_{2,1}-\omega_{1,2})t - \omega_{2,1}\tau, \quad (3)$$

where E and N are the slowly varying complex electric-field amplitude and the carrier density of the semiconductor lasers, respectively. The subscripts 1 and 2 represent lasers 1 and 2, respectively. G_N is the gain coefficient, N_0 is the carrier density at transparency, ϵ is the gain saturation coefficient, and α is the linewidth enhancement factor. τ_p and τ_s are the photon and carrier lifetimes, respectively. $J = 1.1J_{th}$ is the injection current of the lasers, where J_{th} is the injection current at the lasing threshold.

The second term in the right-hand side of Eq. (1) represents the optical injection from the other laser. κ is the coupling strength between the two lasers, and τ is the propagation delay time of the light. $\theta_{1,2}(t)$ is the optical phase difference between the laser light and the injected light. In Eq. (3), $\Delta\omega(=\omega_1-\omega_2)$ is the optical angular frequency detuning between lasers 1 and 2, where ω is the initial optical angular frequency of the laser. $\Delta\omega$ is given by $\Delta\omega = 2\pi\Delta f_{\rm ini}$, where $\Delta f_{\rm ini}$ represents the initial optical frequency detuning between the two lasers, defined as $\Delta f_{\rm ini} = f_{\rm ini1} - f_{\rm ini2}$. The initial optical frequency of laser 1 $f_{\rm ini1}$ is calculated as $f_{\rm ini1} = c/\lambda_1$ from the speed of light c and the optical wavelength λ_1 of laser 1.

The initial optical frequency detuning $\Delta f_{\rm ini}$ and the coupling strength κ are important parameters for observing synchronization in mutually coupled lasers, since they are related to optical injection locking. Injection locking can be achieved for $\Delta f_{\rm ini}$ close to zero and a large κ. In our numerical simulation, κ is fixed at 30.0 ns^{-1} and $\Delta f_{\rm ini}$ is varied.

TABLE I. Parameter values used in numerical simulations.

Symbol	Parameter	Value
G_N	Gain coefficient	8.40×10^{-13} m^3 s^{-1}
N_0	Carrier density at transparency	1.40×10^{24} m^{-3}
ϵ	Gain saturation coefficient	4.5×10^{-23}
τ_p	Photon lifetime	1.927×10^{-12} s
τ_s	Carrier lifetime	2.04×10^{-9} s
α	Linewidth enhancement factor	3.0
λ_1	Optical wavelength of laser 1	1.537×10^{-6} m
c	Speed of light	2.998×10^{8} ms^{-1}
κ	Injection strength	30.00×10^{-9} s^{-1}
$j = J/J_{th}$	Normalized injection current	1.1
τ	Propagation delay time of light between the two lasers	36.64×10^{-9} s
$\Delta f_{\rm ini}$	Initial optical frequency detuning between the two lasers	Variable

The propagation delay time τ is also an important parameter for the dynamics of coupled lasers. In mutually coupled lasers, it has been shown that the temporal output of one laser is synchronized to that of the other laser with τ [24,27]. We use a propagation delay time of $\tau = 36.64$ ns in our numerical simulations, which corresponds to our experimental conditions discussed in Sec. IV. The parameter values used in our numerical simulations are shown in Table I.

B. Global leader-laggard relationship

We observe the temporal dynamics of mutually coupled semiconductor lasers in the LFF regime and investigate the global leader-laggard relationship, which represents the leader and laggard lasers on average for a long duration. Cross-correlation values between the output intensities of lasers 1 and 2 are used to identify the global leader-laggard relationship. We investigate the dependence of the leader-laggard relationship on the optical frequency detuning $\Delta f_{\rm ini}$.

Figure 2(a) shows the temporal wave forms of the laser intensities in mutually coupled semiconductor lasers. The intensities of lasers 1 and 2 are given by $I_{1,2}(t) = |E_{1,2}(t)|^2$. The initial optical frequency detuning is fixed to $\Delta f_{\rm ini} = 2$ GHz. The temporal wave forms shown in Fig. 2(b) are obtained by filtering the temporal wave forms of Fig. 2(a) using a low-pass filter with a cutoff frequency of 0.1 GHz. We use a finite impulse response filter realized by a Hanning window with a window size of 10 ns [46]. A sudden decrease in the intensity, which is called an intensity dropout, is observed in Fig. 2(b). The intensity gradually recovers after the intensity dropout. The interval of the increase in the recovery process corresponds to the round-trip propagation time of light between the two lasers ($2\tau = 73.28$ ns). The intensity dropout and the gradual recovery are evidence of LFF dynamics. The intensity dropout of laser 2 is delayed with a propagation of $\tau = 36.64$ ns compared with that of laser 1. The time lag of the dropouts in Fig. 2(b) indicates that laser 1 is the leader and laser 2 is the laggard.

To identify the leader-laggard relationship, we calculate the cross-correlation function between the temporal wave forms of the laser 1 and 2 intensities as follows:

$$C(\tau_0) = \frac{\langle[I_1(t-\tau_0)-\bar{I}_1][I_2(t)-\bar{I}_2]\rangle_T}{\sigma_1\sigma_2}, \quad (4)$$

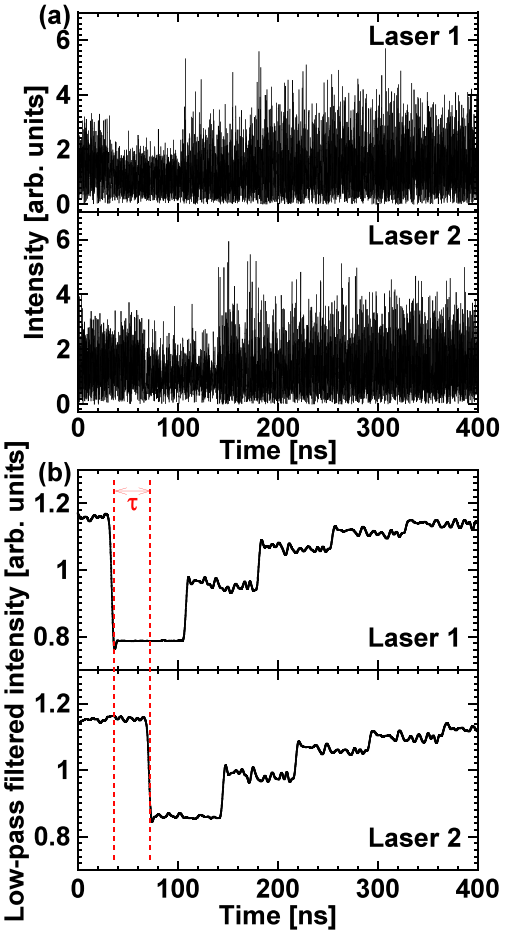

FIG. 2. (a) Temporal wave forms of the laser intensities $I_{1,2}(t)$ in the mutually coupled semiconductor lasers. The initial optical frequency detuning Δf_{ini} is set to 2 GHz. (b) Low-pass-filtered temporal wave forms of (a) with a cutoff frequency of 0.1 GHz.

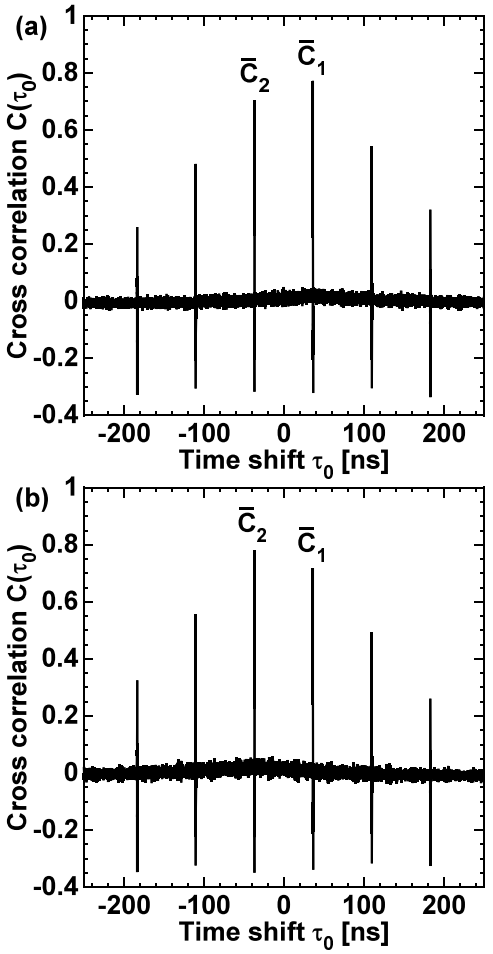

FIG. 3. Cross-correlation function of the temporal wave forms of the two laser intensities. The initial optical frequency detuning is (a) 2 GHz and (b) −2 GHz. The propagation delay time is $\tau = 36.64$ ns.

where the subscripts 1 and 2 represent lasers 1 and 2, respectively. $I_1(t)$ and $I_2(t)$ are the temporal wave forms of the intensities of lasers 1 and 2. $\bar{I}$ is the mean value of the laser intensity for the duration T. σ is the standard deviation of the intensity for T. $\langle\cdot\rangle_T$ represents time averaging over the period T. The cross-correlation function converges for a large value of T. In our study, we used the original temporal wave forms of the laser intensities $I_{1,2}(t)$ for the calculation of the cross-correlation function without using a low-pass filter.

Temporal wave forms with length $T = 10\,000$ ns are used for the calculation of the cross-correlation function. The duration of the intensity dropout and the recovery process is about 400 ns. Therefore, a temporal wave form of 10 000 ns includes ∼25 intensity dropouts.

Figures 3(a) and 3(b) show the cross-correlation function of the temporal wave forms of the two laser intensities for the initial optical frequency detunings of 2 and −2 GHz, respectively. The peak intervals of the cross-correlation function correspond to $2\tau = 73.28$ ns, indicating that the dominant frequency of the delay-coupled laser dynamics is determined by $1/(2\tau)$, as reported in [17]. More importantly, several peaks appear at the delay time of $\pm\tau$, $\pm 3\tau$, $\pm 5\tau$, and so on. The correlation peaks at $\pm\tau$ ($= \pm 36.64$ ns) indicate that one of the two temporal wave forms is shifted by the propagation delay time τ.

Here, we focus on the cross-correlation values at $\tau_0 = \tau$ and $\tau_0 = -\tau$ and refer to them as $\bar{C}_1$ and $\bar{C}_2$, respectively (see Fig. 3). The leader-laggard relationship can be identified from the values of $\bar{C}_1$ and $\bar{C}_2$. It is expected that the delayed signal of the leader laser and the signal of the laggard laser are strongly correlated since the leader laser oscillates earlier than the laggard laser by τ. Therefore, $\bar{C}_1 > \bar{C}_2$ indicates that laser 1 is the leader and $\bar{C}_1 < \bar{C}_2$ indicates that laser 2 is the leader.

In Fig. 3(a), $\bar{C}_1 > \bar{C}_2$ is observed and laser 1 is the leader for the initial optical frequency detuning of 2 GHz. On the contrary, in Fig. 3(b), $\bar{C}_1 < \bar{C}_2$ is observed and the laser 2 is the leader for the detuning of −2 GHz. The role of the leader-laggard is exchanged by changing the sign of the initial optical frequency detuning. The leader-laggard relationship can be identified by comparing the values of $\bar{C}_1$ and $\bar{C}_2$.

We also calculate the optical frequency detuning between lasers 1 and 2 under the mutual coupling Δf_{mc} as follows [47]:

$$\Delta f_{mc}(t) = \Delta f_{\text{ini}} + \frac{1}{2\pi}\frac{\Delta\phi(t) - \Delta\phi(t-T)}{T}, \tag{5}$$

$$\Delta\phi(t) = \phi_1(t) - \phi_2(t), \tag{6}$$

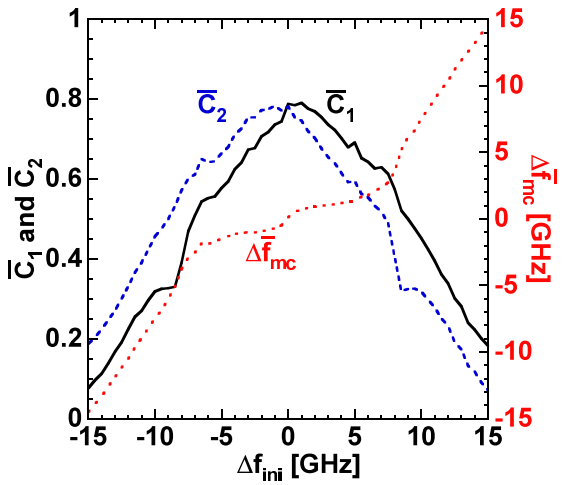

FIG. 4. Averaged cross-correlation values $\bar{C}_1$ (black solid curve), $\bar{C}_2$ (blue dashed curve), and optical frequency detuning under the mutual coupling $\Delta\bar{f}_{mc}$ (red dotted curve) as a function of the initial optical frequency detuning $\Delta f_{\rm ini}$.

where $\Delta\phi(t)$ is the optical phase difference between the two lasers. $\phi(t)$ is calculated as $\phi(t) = \tan^{-1}[E_{im}(t)/E_{re}(t)]$, where $E_{re}(t)$ and $E_{im}(t)$ are the real and imaginary parts of $E(t)$, respectively. The optical frequency detuning $\Delta f_{mc}(t)$ also converges by using a large value of T, defined as $\Delta\bar{f}_{mc}$. We can determine injection locking by using $\Delta\bar{f}_{mc}$ in the mutually coupled lasers. The injection locking occurs under the condition $\Delta\bar{f}_{mc} \approx 0$. When the injection locking does not occur, $\Delta\bar{f}_{mc}$ is nearly equal to $\Delta f_{\rm ini}$.

Figure 4 shows the dependence of the cross-correlation values $\bar{C}_{1,2}$ and the optical frequency detuning $\Delta\bar{f}_{mc}$ on the initial optical frequency detuning $\Delta f_{\rm ini}$. The black solid and blue dashed curves represent $\bar{C}_1$ and $\bar{C}_2$, respectively. The red dotted curve represents $\Delta\bar{f}_{mc}$. For the red dotted curve, $\Delta\bar{f}_{mc}$ in $|\Delta f_{\rm ini}| \leqslant 7.0$ GHz is close to zero due to partial injection locking. In this region, the cross-correlation values $\bar{C}_1$ and $\bar{C}_2$ have relatively large values ranging from 0.5 to 0.8. From the comparison of $\bar{C}_1$ and $\bar{C}_2$, it is found that $\bar{C}_1$ is larger than $\bar{C}_2$ for positive $\Delta f_{\rm ini}$ ($f_{\rm ini1} > f_{\rm ini2}$), while $\bar{C}_2$ is larger than $\bar{C}_1$ for negative $\Delta f_{\rm ini}$ ($f_{\rm ini1} < f_{\rm ini2}$). Thus, laser 1 is the leader for $f_{\rm ini1} > f_{\rm ini2}$ and laser 2 is the leader for $f_{\rm ini1} < f_{\rm ini2}$. This result indicates that the laser with the higher initial optical frequency becomes the global leader. This result is consistent with a previous report in the literature [17].

C. Local leader-laggard relationship

In this section, we investigate temporal changes in the leader-laggard relationship in mutually coupled lasers for a short period. We calculate the short-term cross-correlation values between time-delayed laser 1 and laser 2 (denoted as C_1), and between laser 1 and time-delayed laser 2 (denoted as C_2), by shifting the propagation delay time τ as follows:

$$C_1(t) = \frac{\langle [I_1(t-\tau) - \bar{I}_1][I_2(t) - \bar{I}_2]\rangle_T}{\sigma_1\sigma_2}, \quad (7)$$

$$C_2(t) = \frac{\langle [I_1(t) - \bar{I}_1][I_2(t-\tau) - \bar{I}_2]\rangle_T}{\sigma_1\sigma_2}, \quad (8)$$

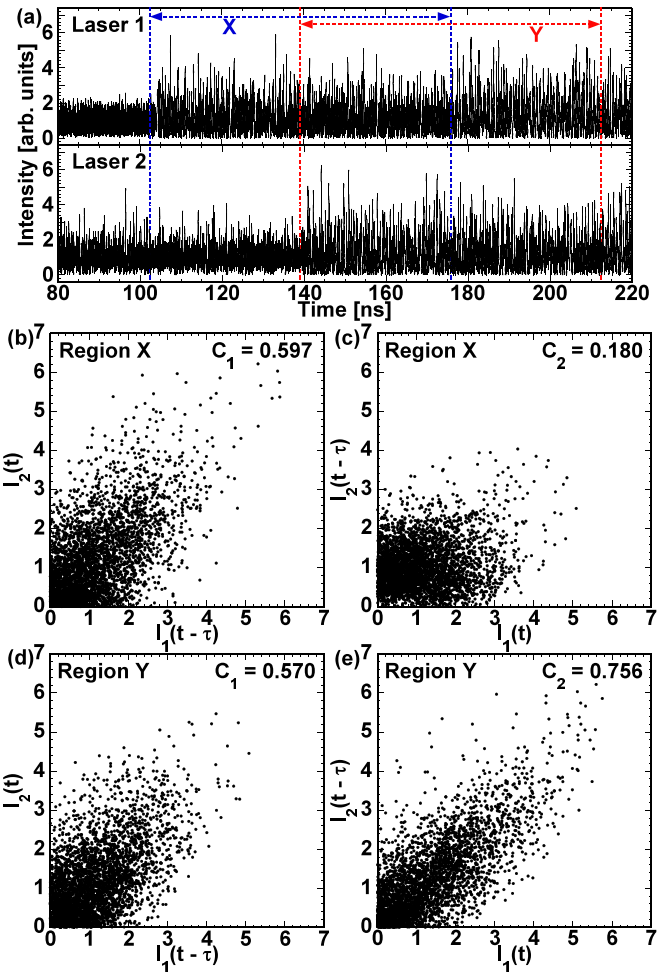

FIG. 5. (a) Temporal wave forms of the laser 1 and 2 intensities at $\Delta f_{\rm ini} = 2$ GHz. (b)–(e) Correlation plots of the two temporal wave forms with a time shift. (b) and (c) are calculated from the temporal wave forms of the region X in (a). (d) and (e) are calculated from the temporal wave forms of the region Y in (a). The temporal wave form of laser 1 is delayed in (b) and (d). The temporal wave form of laser 2 is delayed in (c) and (e).

where $C_1(t)$ is the cross-correlation value between $I_1(t-\tau)$ and $I_2(t)$, and $C_2(t)$ is the cross-correlation value between $I_1(t)$ and $I_2(t-\tau)$. The propagation delay time $\tau = 36.64$ ns is used as the time T for calculating the short-term cross-correlation values. We can observe temporal changes in their correlation values for the short time scale of $T = \tau$. $C_1(t)$ and $C_2(t)$ are converged to $\bar{C}_1$ and $\bar{C}_2$ for a large value of T, as already shown in Figs. 3 and 4. Similar to $\bar{C}_1$ and $\bar{C}_2$, the leader-laggard relationship can be identified from the sign of $\Delta C(t) = C_1(t) - C_2(t)$, i.e., $C_1(t) > C_2(t)$ ($\Delta C(t) > 0$) indicates that laser 1 is the leader and $C_1(t) < C_2(t)$ ($\Delta C(t) < 0$) indicates that laser 2 is the leader.

Figure 5(a) shows the temporal wave forms of the laser 1 and 2 intensities, and is an enlarged view of Fig. 2(a). The correlation plots shown in Figs. 5(b)–5(e) are obtained from the temporal wave forms in the time windows X and Y with a width of 2τ in Fig. 5(a). In these correlation plots, one of the two lasers is delayed by τ. Thus, the first half of one temporal wave form and the second half of the other wave form in

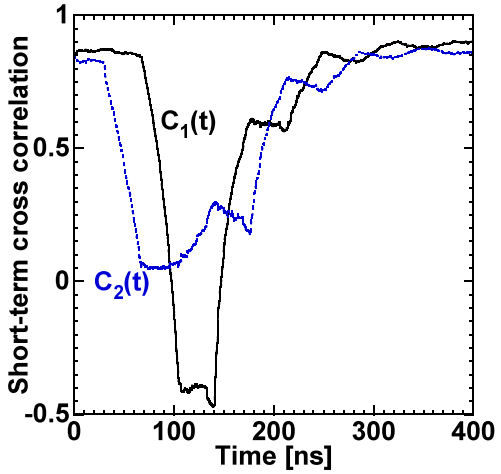

FIG. 6. Temporal wave forms of the short-term cross-correlation values $C_{1,2}(t)$ and the short-term optical frequency detuning under the mutual coupling $\Delta f_{mc}(t)$. The initial optical frequency detuning is set to $\Delta f_{\text{ini}} = 2$ GHz. The black solid and blue dashed curves are $C_1(t)$ and $C_2(t)$, respectively.

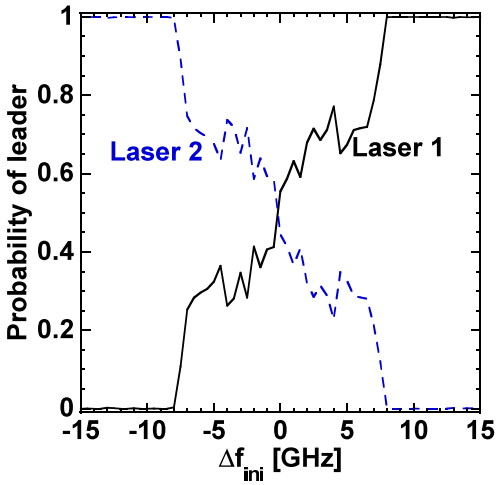

FIG. 7. Probability of being the local leader as a function of the initial optical frequency detuning Δf_{ini}. Laser 1 is the local leader when $C_1(t) - C_2(t) > C_{th}$, whereas laser 2 is the local leader when $C_2(t) - C_1(t) > C_{th}$, where $C_{th} = 0.1$. The black solid and blue dashed curves represent the probabilities of the local leader being lasers 1 and 2, respectively.

the windows are used for calculating the correlation plots. Figures 5(b) and 5(c) are the correlation plots for window X in Fig. 5(a). The laser 1 and 2 intensities are delayed by τ for Figs. 5(b) and 5(c), respectively. Delayed laser 1 and laser 2 in Fig. 5(b) are more highly correlated than the case of laser 1 and delayed laser 2 in Fig. 5(c). The short-term cross-correlation values are $C_1(t) = 0.597$ and $C_2(t) = 0.180$ for Figs. 5(b) and 5(c), respectively. Laser 1 is the local leader, since $C_1(t)$ is larger than $C_2(t)$. Figures 5(d) and 5(e) are the correlation plots in window Y, which is shifted from window X by τ. The cross-correlation values are $C_1(t) = 0.570$ and $C_2(t) = 0.756$ for Figs. 5(d) and 5(e), respectively. Laser 2 becomes the local leader since $C_2(t)$ is larger than $C_1(t)$. Although $C_1(t)$ hardly changes between windows X and Y, $C_2(t)$ increases and exceeds $C_1(t)$, showing that the local leader-laggard relationship is exchanged.

We show the temporal behavior of the short-term cross-correlation values $C_1(t)$ and $C_2(t)$ in Fig. 6. The dynamics of the mutually coupled lasers operate in the LFF regime. The temporal wave forms of $C_1(t)$ and $C_2(t)$ for an intensity dropout and a recovery process in LFFs are shown in Fig. 6. The initial optical frequency detuning is set to $\Delta f_{\text{ini}} = 2$ GHz. Thus, laser 1 is considered the global leader and has an intensity dropout earlier than laser 2. In Fig. 6, $C_2(t)$ starts decreasing at about 30 ns, which results from the intensity dropout of laser 1. The decrease of $C_1(t)$ is delayed by the propagation delay time $\tau = 36.64$ ns, because the intensity dropout of laser 2 is delayed by τ from the dropout of laser 1. After $C_1(t)$ and $C_2(t)$ decrease, their cross-correlation values alternately increase. The sign of $\Delta C(t) = C_1(t) - C_2(t)$ changes repeatedly, which indicates that the local leader-laggard relationship is exchanged. Although laser 1 always shows an earlier intensity dropout than laser 2 due to the positive value of Δf_{ini}, the local leader-laggard relationship is exchanged spontaneously during the recovery process of LFF. The intervals of the spontaneous exchanges correspond to the propagation delay time τ.

We investigate the dependence of the spontaneous exchange of the local leader-laggard relationship on the initial optical frequency detuning Δf_{ini}. To quantitatively evaluate the spontaneous exchange, we calculate the probability of the duration for which one of the lasers becomes the leader. The local leader-laggard relationship is identified from $\Delta C(t)$, where $\Delta C(t) > C_{th}$ or $\Delta C(t) < C_{th}$ indicates laser 1 or 2 is the local leader, respectively. $C_{th} = 0.1$ is used to exclude the ambiguity of the local leader-laggard relationship near $\Delta C(t) \approx 0$.

Figure 7 shows the probability of being the local leader as a function of the initial optical frequency detuning Δf_{ini}. The black solid and blue dashed curves represent the probability of the local leader being laser 1 and 2, respectively. For $|\Delta f_{\text{ini}}| > 8$ GHz, the probability is almost 1 or zero, which indicates that one of the two lasers always becomes the leader. Therefore, spontaneous exchange is not observed for $|\Delta f_{\text{ini}}| > 8$ GHz. For $|\Delta f_{\text{ini}}| < 8$ GHz, the probability of the leader for each laser is not zero, which indicates that the leader laser changes in time. Therefore, small $|\Delta f_{\text{ini}}|$ leads to spontaneous exchange of the leader-laggard relationship. Comparing Fig. 7 with Fig. 4, it is found that the parameter region for the spontaneous exchange roughly corresponds to the region with small $\Delta \bar{f}_{mc}$ due to partial injection locking. This result indicates that spontaneous exchange occurs under partial injection locking.

The occurrence of the spontaneous exchange is related to the dynamics of the mutually coupled lasers. Figures 8(a) and 8(b) show the low-pass-filtered temporal wave forms of the laser intensities. The initial optical frequency detunings Δf_{ini} for Figs. 8(a) and 8(b) are set to 5 GHz and 10 GHz, respectively. Intensity dropouts are observed in Fig. 8(a), which indicates LFF dynamics. The dynamics shows the transition between the LFF and coherent collapse regimes, which results in a large number of intensity dropouts [48], since gradual recovery is not clearly observed. In Fig. 8(b), there is no intensity dropout, and the dynamics is fully developed coherent collapse. The temporal wave forms of $C_1(t)$ and $C_2(t)$ are shown

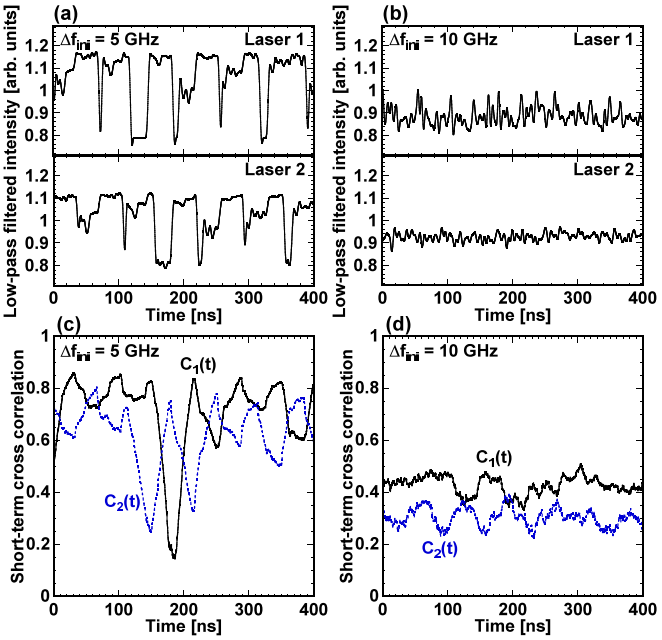

FIG. 8. (a), (b) Low-pass-filtered temporal wave forms of the laser intensities. The initial optical frequency detunings $\Delta f_{\rm ini}$ are 5 GHz and 10 GHz for (a) and (b), respectively. (c), (d) Temporal wave forms of the short-term cross-correlation values $C_{1,2}(t)$ corresponding to (a) and (b). The black solid and blue dashed curves represent $C_1(t)$ and $C_2(t)$, respectively.

in Figs. 8(c) and 8(d), corresponding to Figs. 8(a) and 8(b), respectively. In Fig. 8(c), $C_1(t)$ and $C_2(t)$ alternatively switch and the sign of $\Delta C(t)$ changes in time, which indicates the occurrence of spontaneous exchange of the leader-laggard relationship. In Fig. 8(d), however, $C_1(t)$ is larger than $C_2(t)$ for most of the time and the sign of $\Delta C(t)$ remains positive. Thus, the spontaneous exchange occurs only in the LFF dynamics but not in the fully developed coherent collapse regime.

III. STEADY-STATE SOLUTIONS OF THE LANG-KOBAYASHI EQUATIONS

In this section, we investigate the mechanism of spontaneous exchange of the leader-laggard relationship. We derive the steady-state solutions of the numerical model for mutually coupled semiconductor lasers. Steady-state solutions are useful for understanding the mechanism of laser dynamics. It is well known that in the LFF dynamics of a semiconductor laser with optical feedback, the trajectory of the laser in phase space itinerates around the steady-state solutions [29,30].

We now determine the steady-state solutions calculated from the Lang-Kobayashi equations (1) and (2) for mutually coupled semiconductor lasers in the presence of an initial optical frequency detuning. We explain the relationship between the steady-state solutions and the trajectories of the lasers that exhibit spontaneous exchange. In Eqs. (1) and (2), we define the steady-state solutions of $E_{1,2}(t)$ and $N_{1,2}(t)$ as $A_{s1,s2}\exp[i(\omega_{s1,s2}-\omega_{1,2})t]$ and $N_{s1,s2}$, respectively. The subscripts $s1$ and $s2$ represent the solutions for lasers 1 and 2, respectively. $A_{s1,s2}$ are the steady-state solutions for the electric-field amplitudes. $\omega_{s1,s2}$ are the steady-state solutions for the optical angular frequencies of the lasers. We consider that $A_{s1,s2}$, $\omega_{s1,s2}$, and $N_{s1,s2}$ are time-constant values. The following equations are obtained by inserting these solutions into Eqs. (1) and (2) and by decomposing complex variables into amplitude and phase terms:

$$0=\frac{1}{2}\left[\frac{G_N(N_{s1,s2}-N_0)}{1+\epsilon|A_{s1,s2}|^2}-\frac{1}{\tau_p}\right]+\kappa\frac{A_{s2,s1}}{A_{s1,s2}}\cos\theta_{1,2}(t), \quad (9)$$

$$\omega_{s1,s2}-\omega_{1,2}=\frac{\alpha}{2}\left[\frac{G_N(N_{s1,s2}-N_0)}{1+\epsilon|A_{s1,s2}|^2}-\frac{1}{\tau_p}\right]-\kappa\frac{A_{s2,s1}}{A_{s1,s2}}\sin\theta_{1,2}(t), \quad (10)$$

$$0=J-\frac{N_{s1,s2}}{\tau_s}-\frac{G_N(N_{s1,s2}-N_0)}{1+\epsilon|A_{s1,s2}|^2}|A_{s1,s2}|^2, \quad (11)$$

$$\theta_{1,2}(t)=(\omega_{s1,s2}-\omega_{s2,s1})t+\omega_{s2,s1}\tau. \quad (12)$$

It is worth noting that $\theta_{1,2}(t)$ need to be time invariant, which is satisfied by assuming $\omega_{s1}=\omega_{s2}$. This assumption corresponds to injection locking between the two lasers. We obtain the following equations for the steady-state solutions from Eqs. (9)–(12) under the assumption $\omega_s=\omega_{s1}=\omega_{s2}$:

$$(\omega_s-\omega_1)(\omega_s-\omega_2)=\kappa^2(1+\alpha^2)\sin^2[\omega_s\tau+\tan^{-1}\alpha], \quad (13)$$

$$N_{s1,s2}-N_{th}=\frac{2\kappa^2\tau_s\sqrt{1+\alpha^2}\cos[\omega_s\tau]\sin[\omega_s\tau+\tan^{-1}\alpha]}{(G_N\tau_s+\epsilon)(\omega_s-\omega_{2,1})}+\frac{\epsilon N_{th}(j-1)}{G_N\tau_s+\epsilon}, \quad (14)$$

$$A_s^2=\frac{jN_{th}-N_s}{\tau_s G_N(N_s-N_0)-\epsilon(N_s-jN_{th})}, \quad (15)$$

where N_{th} is the carrier density at the lasing threshold $[N_{th}=N_0+1/(G_N\tau_p)]$. $j=J/J_{th}$ is the normalized injection current and $J_{th}=N_{th}/\tau_s$ is the injection current at the lasing threshold. The steady-state solutions ω_s and $N_{s1,s2}$ are obtained by numerically solving Eqs. (13) and (14) with a root-finding algorithm.

The following parameter values are used to calculate the solutions: propagation delay time $\tau=5$ ns, coupling strength $\kappa=31.06\ \text{ns}^{-1}$, initial optical frequency detuning $\Delta f_{\rm ini}=2$ GHz, and gain saturation parameter $\epsilon=2.0\times10^{-23}$. We use a delay time smaller than that in our numerical simulations to avoid too many steady-state solutions. The other parameter values are the same as those in Table I.

We consider a nonzero value of the initial optical frequency detuning $\Delta f_{\rm ini}\neq0$ $(\omega_1\neq\omega_2)$. The steady-state solutions obtained by Eqs. (13)–(15) are different from the complete synchronized solutions in the case of $\Delta f_{\rm ini}=0$ reported in Ref. [49]. The steady-state solutions of Eqs. (13)–(15) become identical to the complete synchronized solutions in Ref. [49] only for the condition $\Delta f_{\rm ini}=0$.

Figure 9(a) represents the steady-state solutions obtained from Eqs. (13) and (14). The vertical axis in Fig. 9(a) is the normalized carrier density calculated as $100N_{s1,s2}/N_{th}$. The horizontal axis is the optical frequency shift $f_s=(\omega_s-\omega_1)/(2\pi)$, which is represented as the steady-state solution of the frequency shifted from the solitary laser 1 $f_{\rm ini1}=\omega_1/(2\pi)$.

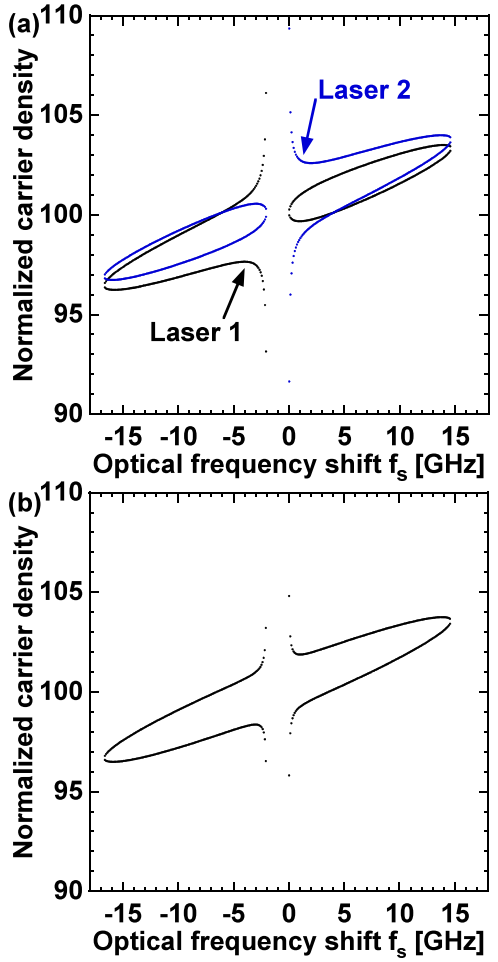

FIG. 9. (a) Steady-state solutions calculated from Eqs. (13) and (14). The black and blue dots represent the steady-state solutions of lasers 1 and 2, respectively. (b) Averaged steady-state solutions between lasers 1 and 2.

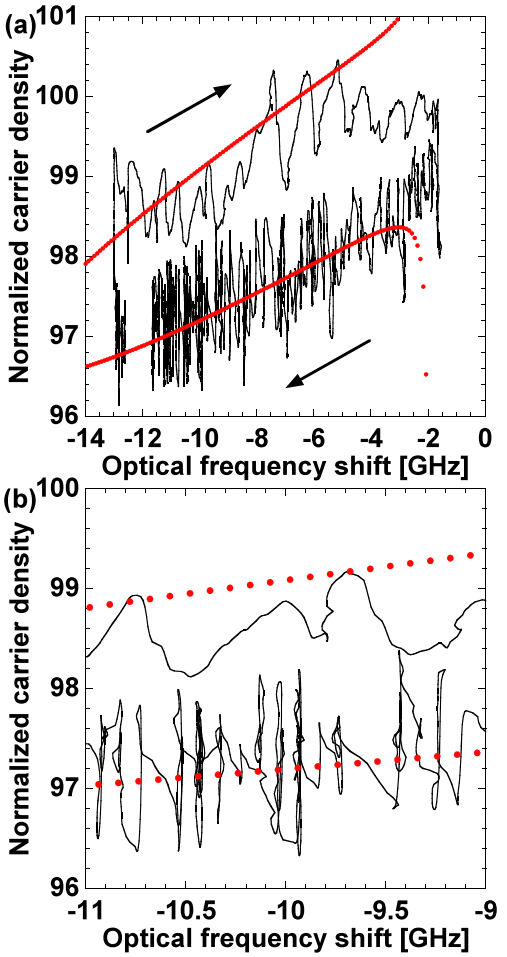

FIG. 10. (a) Averaged steady-state solutions (red dots) and averaged trajectory (black curve) in the phase space of the optical frequency shift and the carrier density. (b) Enlarged view of (a).

The black and the blue dots represent the steady-state solutions for lasers 1 and 2, respectively. Asymmetric distributions of the steady-state solutions of the two lasers are found with respect to the optical frequency shift. Figure 9(b) shows the averaged steady-state solutions for the two lasers. The averaged steady-state solutions are distributed symmetrically.

We consider the averaged trajectory of the two lasers in order to understand the mechanism of the spontaneous exchange of the leader-laggard relationship. The averaged trajectory for mutually coupled semiconductor lasers with optical feedback has been investigated from the viewpoint of synchronization in Ref. [49]. We calculate the averaged trajectory of the carrier density as $100N_A(t)/N_{th}$, where $N_A(t) = [N_1(t) + N_2(t)]/2$. We calculate the averaged optical frequency of the two lasers $f_A(t) = [f_1(t) + f_2(t)]/2$, where $f_{1,2}(t)$ are the optical frequency shifts calculated from $f_1(t) = [\phi_1(t) - \phi_1(t-\tau)]/(2\pi\tau)$ and $f_2(t) = [\phi_2(t) - \phi_2(t-\tau)]/(2\pi\tau) - \Delta f_{\rm ini}$.

Figure 10 shows the averaged trajectory (black curve) for lasers 1 and 2, and the steady-state solutions (red dots) projected on the phase space of the carrier density and the optical frequency shift. The averaged trajectory shown in Fig. 10 includes an intensity dropout and a gradual recovery in LFF dynamics. In Fig. 10(a), the trajectory moves in a clockwise fashion. The carrier density suddenly increases from the lower side to the upper side of the steady-state solutions at $f_A(t) \approx -13$ GHz, which corresponds to an intensity dropout. After the increase of the carrier density, the trajectory moves toward $f_A(t) \approx 0$. The trajectory then drifts toward the negative direction of the optical frequency along the solutions of the lower side. Figure 10(b) shows an enlarged view of the averaged trajectory. It is worth noting that the averaged trajectory itinerates on the averaged steady-state solutions chaotically toward the direction of negative optical frequencies. This phenomenon is considered as chaotic itinerancy of the averaged trajectory.

We now calculate the temporal wave forms of the optical frequencies $f_{1,2,A}(t)$ and investigate the relationship between the optical frequencies and the short-term cross-correlation values $C_{1,2}(t)$. Figure 11(a) shows the temporal wave forms of the individual optical frequency $f_1(t)$, $f_2(t)$, and their averaged value $f_A(t)$. The averaged trajectory corresponds to $f_A(t)$ in Fig. 10. The vertical dashed lines indicate the times when one of the optical frequencies $f_{1,2}(t)$ starts decreasing, and the interval of the lines equals the propagation delay time

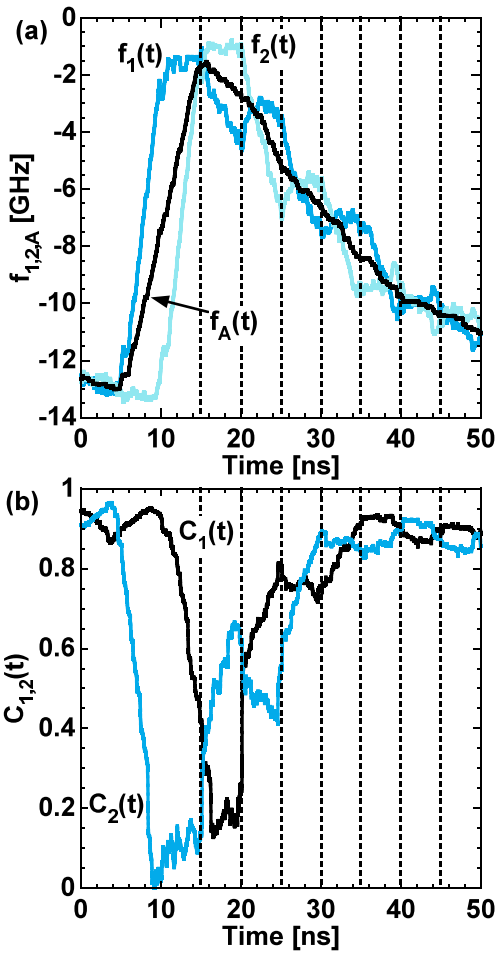

FIG. 11. (a) Time evolution of the optical frequency shifts $f_{1,2,A}(t)$. The black, cyan blue (dark gray), and sky blue (light gray) curves represent $f_A(t)$, $f_1(t)$, and $f_2(t)$, respectively. The vertical dashed lines are drawn with the interval of the propagation delay time ($\tau = 5$ ns) from 15 ns. (b) Time evolution of the short-term cross-correlation values $C_1(t)$ and $C_2(t)$. The black and cyan blue (dark gray) curves represent $C_1(t)$ and $C_2(t)$, respectively.

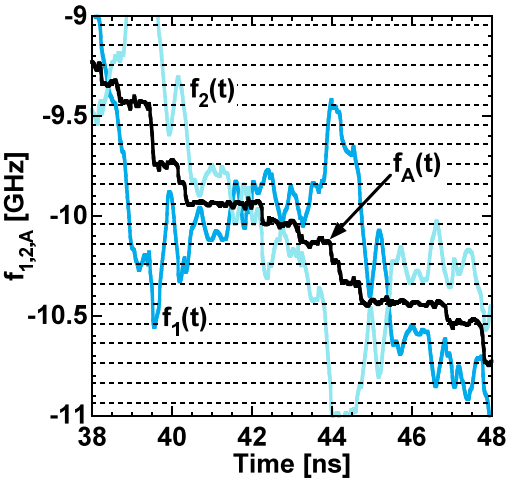

FIG. 12. Enlarged view of Fig. 11(a). The black, cyan blue (dark gray), and sky blue (light gray) curves represent $f_A(t)$, $f_1(t)$, and $f_2(t)$, respectively. The horizontal dashed lines represent the averaged steady-state solutions of the optical frequency in the lower side of Fig. 10(b).

$\tau = 5$ ns. The individual optical frequencies $f_1(t)$ and $f_2(t)$ change differently in time, which results from the lack of zero-lag synchronization solutions in the presence of the initial optical frequency detuning $\Delta f_{\rm ini} = 2$ GHz. For example, $f_1(t)$ starts increasing at 5 ns, which indicates an intensity dropout of laser 1. $f_2(t)$ also starts increasing at 10 ns, while $f_1(t)$ is almost constant until 15 ns. $f_1(t)$ starts decreasing at 15 ns and $f_2(t)$ hardly changes, which leads to $f_2(t) > f_1(t)$ until 20 ns. After that, $f_1(t)$ increases and $f_2(t)$ decreases during the period from 20 ns to 25 ns, and the relationship between $f_1(t)$ and $f_2(t)$ is reversed [$f_1(t) > f_2(t)$]. This process is repeated for every 5-ns durations.

The switching between $f_1(t)$ and $f_2(t)$ is related to the optical frequencies of the injected light into each laser. The optical frequency of the injected light into laser 1 corresponds to $f_2(t-\tau)$, since the injected light is delayed by the propagation delay time $\tau = 5$ ns. For laser 2, the optical frequency of the injected light into laser 2 corresponds to $f_1(t-\tau)$. For example, in Fig. 11(a), $f_2(t)$ decreases rapidly from 20 to 25 ns, since $f_2(t)$ is strongly affected by $f_1(t-\tau)$ and $f_1(t)$ decreases from 15 to 20 ns. However, $f_1(t)$ does not change much from 20 to 25 ns since it is affected by $f_2(t-\tau)$, and $f_2(t)$ stays almost constant from 15 to 20 ns. After 5 ns, the relationship between $f_1(t)$ and $f_2(t)$ is reversed, i.e., $f_2(t)$ stays constant and $f_1(t)$ decreases rapidly from 25 to 30 ns, since they are affected by $f_1(t-\tau)$ and $f_2(t-\tau)$, respectively.

The local leader-laggard relationship can be determined from Fig. 11(b), which shows the dynamics of the short-term cross-correlations $C_1(t)$ and $C_2(t)$. From 20 to 25 ns, $C_1(t)$ is larger than $C_2(t)$, indicating that laser 1 is the leader and laser 2 is the laggard. This observation is consistent with the fact that $f_2(t)$ is pulled by $f_1(t-\tau)$ in Fig. 11(a). Compared with Figs. 11(a) and 11(b), when $f_i(t)$ ($i = 1$ or 2) decreases more rapidly than the frequency of the other laser, laser i becomes the laggard, since it follows the frequency and dynamics of the other laser. $f_i(t)$ decreases more than the frequency of the other laser for the period of τ, and the switching of the leader-laggard relationship occurs every τ due to the delayed optical injection.

It is known that it is easier to transfer the optical power to lower-frequency external-cavity modes in semiconductor lasers [29]. The energy in each mode is transferred to the lower-frequency side as a result of the anomalous interaction of lasing modes [50], since the lower-frequency mode acquires excess gain in the presence of multimodes. Therefore, the frequency of the laser tends to be pulled by injected light of lower frequency. This phenomenon explains the mechanism for which the laser subjected to the injected light of lower frequency becomes the laggard.

Figure 12 shows the dynamics of $f_1(t)$, $f_2(t)$, and their average $f_A(t)$ [enlarged view of Fig. 11(a)]. The steady-state solutions for the optical frequency are shown as the horizontal dashed lines. It is worth noting that the averaged optical frequency $f_A(t)$ is locked on the steady-state solutions and slipped toward the negative frequency direction, whereas $f_1(t)$ and $f_2(t)$ fluctuate chaotically without frequency locking. We

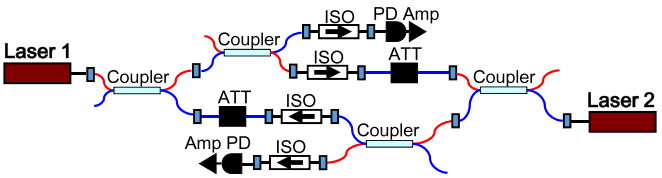

FIG. 13. Experimental setup of mutually coupled semiconductor lasers. Amp, electric amplifier; ATT, attenuator; ISO, optical isolator; PD, photodetector.

interpret that the partial frequency locking of $f_A(t)$ always occurs, and the change in $f_1(t)$ and $f_2(t)$ determines the local leader-laggard relationship, i.e., the laser with a rapid decrease of the optical frequency in the negative direction corresponds to the laggard. This observation may be slightly shifted from the local leader-laggard relationship determined by the cross-correlation values, since there is a small time lag in the synchronization of the temporal wave forms after the switching occurs.

IV. EXPERIMENTAL RESULTS

A. Experimental setup

We experimentally investigate the spontaneous exchange of the leader-laggard relationship of the mutually coupled semiconductor lasers to verify our numerical results. Figure 13 shows our experimental setup of the mutually coupled semiconductor lasers. We used two distributed-feedback (DFB) semiconductor lasers (NTT Electronics, NLK1C5GAAA), which have an optical wavelength of 1547 nm (referred to as lasers 1 and 2). The lasers were prepared without standard optical isolators to allow optical injection. The lasers were mutually coupled through two optical passes, which were constructed to form a symmetric coupling configuration. Each pass provided unidirectional coupling from one laser to the other by using an optical isolator (ISO). The optical injection strengths of the two optical passes were adjusted by using the attenuators. The fiber lengths between the two lasers were 15.22 m, which corresponds to the propagation delay time of $\tau = 36.64$ ns. The optical outputs of the lasers were divided by fiber couplers (FC) and converted into electric signals by photodetectors (PD, New Focus, 1554-B) with a frequency bandwidth of 12 GHz. The electrical signals were amplified by noninverting traveling wave amplifiers (Amp, New Focus, 1422-LF) with high-pass and low-pass cutoff frequencies of 14 MHz and 20 GHz, respectively. The amplified electric signals were sent to a digital oscilloscope (Tektronix, DPO71604B, 16 GHz bandwidth, 50 GigaSamples/s). An optical spectrum analyzer (Yokogawa, AQ6370B) was used to measure the optical wavelengths of the lasers. Polarization-maintaining fibers were used for all the optical fiber components.

The injection current and the temperature of the lasers were adjusted using a current-temperature controller. The lasing thresholds of the injection currents for lasers 1 and 2 were 8.02 mA and 9.91 mA, respectively. The injection currents were set to 8.82 mA and 10.90 mA, respectively (1.1 times the lasing thresholds for both of the lasers). The relaxation oscillation frequencies of solitary lasers 1 and 2 were 1.25 GHz and 1.11 GHz, respectively. The optical wavelengths of the solitary lasers were precisely controlled by the temperature of the lasers. In our experiment, the peak wavelength λ_1 of solitary laser 1 was fixed to 1 547.045 nm by adjusting the laser temperature to 294.01 K. The peak wavelength λ_2 of solitary laser 2 was changed to vary the optical frequency detuning between the two lasers $\Delta f_{\rm ini}$, which is given by $\Delta f_{\rm ini} = c/\lambda_1 - c/\lambda_2$. The temperature of laser 2 was set to be 295.20 K under the condition $\lambda_2 = \lambda_1$ ($\Delta f_{\rm ini} = 0$). The optical powers injected into lasers 1 and 2 were 28.5 μW and 49.5 μW, respectively, to give the same values of $\bar{C}_1$ and $\bar{C}_2$ at $\Delta f_{\rm ini} = 0$.

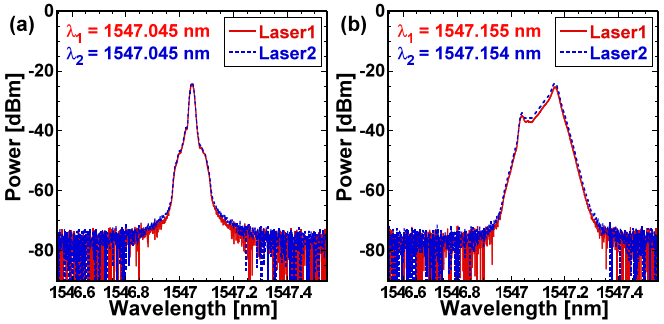

FIG. 14. Experimentally obtained optical spectra of lasers 1 and 2 when the two lasers are (a) not coupled and (b) mutually coupled. The initial optical frequency detuning is set to $\Delta f_{\rm ini} = 0$ GHz.

B. Global leader-laggard relationship

We experimentally investigate the dependence of the global leader-laggard relationship on the initial optical frequency detuning $\Delta f_{\rm ini}$. The global leader-laggard relationship is identified from the comparison between $\bar{C}_1$ and $\bar{C}_2$. The cross-correlation values $\bar{C}_{1,2}$ are calculated from Eq. (4). The

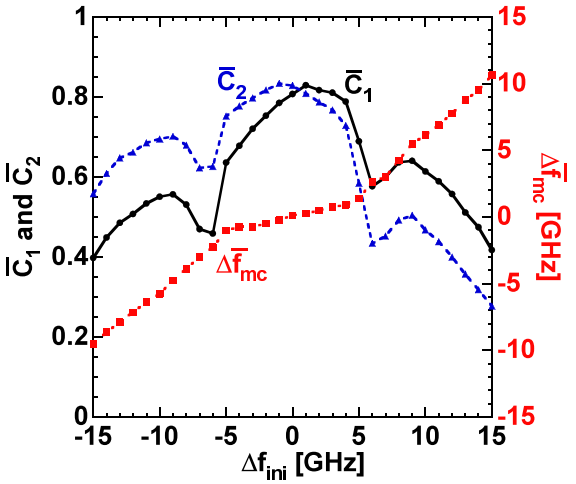

FIG. 15. Experimentally obtained cross-correlation values $\bar{C}_{1,2}$ and optical frequency detuning under the mutual coupling $\Delta \bar{f}_{mc}$ as a function of the initial optical frequency detuning $\Delta f_{\rm ini}$. The black solid curve with circles and the blue dashed curve with triangles represent $\bar{C}_1$ and $\bar{C}_2$, respectively. The red dotted curve with squares represents $\Delta \bar{f}_{mc}$.

delay time for the calculation of $\bar{C}_{1,2}$ is set to $\tau = 36.64$ ns. The averaging time T for the correlation values is 60 000 ns.

We investigate the dependence of the optical frequency detuning under the mutual coupling on $\Delta f_{\rm ini}$. The optical spectra of the two lasers without and with the mutual coupling are shown in Figs. 14(a) and 14(b), respectively. The initial optical frequency detuning $\Delta f_{\rm ini}$ is set to zero, which is achieved by matching the peak wavelengths of the two lasers as shown in Fig. 14(a). Figure 14(b) shows the optical spectra when the lasers are mutually coupled. From these spectra, we calculate the weighted means of the optical wavelengths $\bar{\lambda}_{1,2}$, where the weights are calculated from the linear scale of the optical spectra. The optical frequency detuning under the mutual coupling $\Delta \bar{f}_{mc}$ is given by $\Delta \bar{f}_{mc} = c/\bar{\lambda}_1 - c/\bar{\lambda}_2$. In Fig. 14(b), $\Delta \bar{f}_{mc}$ of 0.038 GHz is obtained. When $\Delta f_{\rm ini}$ is small, $\Delta \bar{f}_{mc}$ becomes nearly equal to zero due to injection locking.

Figure 15 shows the cross-correlation values $\bar{C}_{1,2}$ and the optical frequency detuning under the mutual coupling $\Delta \bar{f}_{mc}$ when the initial optical frequency detuning $\Delta f_{\rm ini}$ is changed. The black solid curve with circles and the blue dashed curve with triangles represent the cross-correlation values $\bar{C}_1$ and $\bar{C}_2$, respectively. When $\Delta f_{\rm ini}$ is positive, $\bar{C}_1$ is larger than $\bar{C}_2$, and laser 1 is the global leader. When $\Delta f_{\rm ini}$ is negative, $\bar{C}_2$ is larger than $\bar{C}_1$, and laser 2 is the global leader. The dependence of $\bar{C}_1$ and $\bar{C}_2$ is almost symmetric with respect to $\Delta f_{\rm ini} = 0$. The red dotted curve with squares represents the optical frequency detuning under the mutual coupling $\Delta \bar{f}_{mc}$. The slopes of $\Delta \bar{f}_{mc}$ inside and outside the region of $|\Delta f_{\rm ini}| \leqslant 5$ GHz are different. The detuning $\Delta \bar{f}_{mc}$ is close to zero in $|\Delta f_{\rm ini}| \leqslant 5$ GHz due to partial injection locking of the optical frequencies. Our experimental result shown in Fig. 15 agrees well with the numerical result shown in Fig. 4.

C. Local leader-laggard relationship

In this section, we show experimental results of the spontaneous exchange of the local leader-laggard relationship. Figure 16 shows an example of the spontaneous exchange. The temporal wave forms of the laser intensities and the short-term cross-correlation values $C_{1,2}(t)$ are shown in Figs. 16(a) and 16(b), respectively. The initial optical frequency detuning $\Delta f_{\rm ini}$ is set to 1 GHz. The lasers operate in the LFF regime and the temporal wave forms of an intensity dropout and a recovery process are shown in Fig. 16(a). Laser 1 exhibits an intensity dropout earlier than laser 2 due to a positive value of $\Delta f_{\rm ini}$ (laser 1 is the global leader). The laser intensity immediately increases after the intensity dropouts; however, gradual recovery is not observed since a low-pass filter is not applied to the temporal wave forms in Fig. 16(a).

The temporal wave forms of the short-term cross-correlation values $C_{1,2}(t)$ are shown in Fig. 16(b) and the spontaneous exchange of the leader-laggard relationship can be observed. $C_2(t)$ starts decreasing when laser 1 experiences an intensity dropout and $C_1(t)$ becomes larger than $C_2(t)$, which indicates that laser 1 is the local leader. The intensity dropout of laser 2 is delayed by the propagation delay time $\tau = 36.64$ ns with respect to laser 1 and $C_1(t)$ starts decreasing. After that, the short-term cross-correlation values exchange alternately in time. Therefore, we experimentally confirm the spontaneous exchange of the leader-laggard relationship.

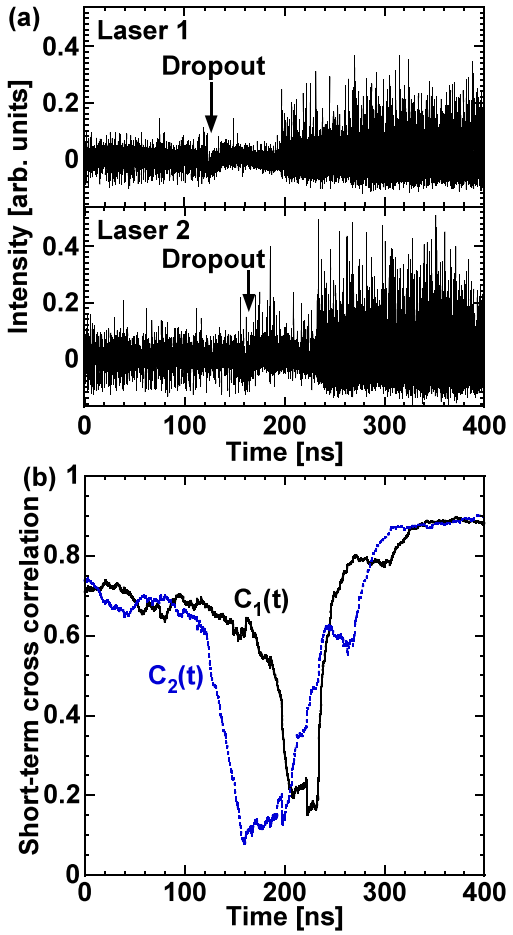

FIG. 16. (a) Experimentally obtained temporal wave forms of the laser intensities. (b) Temporal wave form of the short-term cross-correlation values $C_{1,2}(t)$, corresponding to (a). The initial optical frequency detuning is set to $\Delta f_{\rm ini} = 1$ GHz.

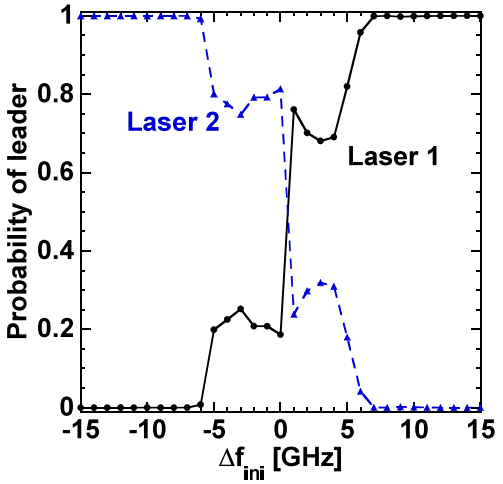

FIG. 17. Experimentally obtained probability of being the local leader as a function of the initial optical frequency detuning $\Delta f_{\rm ini}$. The black solid curve with circles and blue dashed curves with triangles represent lasers 1 and 2, respectively.

Finally, we investigate the dependence of the spontaneous exchange of the local leader-laggard relationship on the initial optical frequency detuning Δf_{ini}. Figure 17 shows the probability of being the local leader as a function of Δf_{ini}, calculated from $C_{1,2}(t)$ by using Eqs. (7) and (8) for $T = \tau$. In the region $|\Delta f_{\mathrm{ini}}| \leqslant 5$ GHz, the probability of being the local leader for lasers 1 and 2 is not zero. Therefore, both lasers 1 and 2 have some probability of being the local leader, and the local leader exchanges in time. On the other hand, only one of the lasers always becomes the leader when $|\Delta f_{\mathrm{ini}}|$ is large. This result agrees well with the numerical results shown in Fig. 7.

V. CONCLUSIONS

We investigated spontaneous exchange of the leader-laggard relationship in mutually coupled semiconductor lasers. The two lasers show LFF dynamics, and one of the lasers, defined as the leader, always experiences intensity dropouts in advance of the other laser, due to the existence of the optical frequency detuning. We observed the spontaneous exchange of the leader-laggard relationship by using short-term cross-correlations. We also calculated the steady-state solutions, which are frequency-locked solutions, for the mutually coupled semiconductor lasers to investigate the mechanism of the spontaneous exchange of the leader-laggard relationship. We found that the averaged trajectory for the two coupled lasers in the phase space itinerates around the steady-state solutions, and partial optical frequency locking alternately occurs in the two lasers. We experimentally confirmed the existence of the spontaneous exchange of the leader-laggard relationship. The spontaneous exchange of the leader-laggard relationship could be a general phenomenon in mutually coupled nonlinear dynamical systems with time delay.

ACKNOWLEDGMENTS

We acknowledge support from a Grant-in-Aid for Scientific Research (KAKENHI Grants No. JP16K16129 and No. JP16H03878) and management expenses grants from the Ministry of Education, Culture, Sports, Science and Technology in Japan.

[1] L. M. Pecora and T. L. Carroll, Phys. Rev. Lett. **64**, 821 (1990).
[2] A. S. Landsman and I. B. Schwartz, Phys. Rev. E **75**, 026201 (2007).
[3] S. Boccaletti, J. Kurths, G. Osipov, D. Valladares, and C. Zhou, Phys. Rep. **366**, 1 (2002).
[4] H. D. I. Abarbanel, N. F. Rulkov, and M. M. Sushchik, Phys. Rev. E **53**, 4528 (1996).
[5] T. U. Singh, A. Nandi, and R. Ramaswamy, Phys. Rev. E **78**, 025205 (2008).
[6] E. A. Rogers, R. Kalra, R. D. Schroll, A. Uchida, D. P. Lathrop, and R. Roy, Phys. Rev. Lett. **93**, 084101 (2004).
[7] M. G. Rosenblum, A. S. Pikovsky, and J. Kurths, Phys. Rev. Lett. **76**, 1804 (1996).
[8] C. Zhou and J. Kurths, Phys. Rev. Lett. **88**, 230602 (2002).
[9] J.-n. Teramae and D. Tanaka, Phys. Rev. Lett. **93**, 204103 (2004).
[10] C. Schafer, Nature (London) **392**, 239 (1998).
[11] W. Singer, Nature (London) **397**, 391 (1999).
[12] A. Argyris, D. Syvridis, L. Larger, V. Annovazzi-Lodi, P. Colet, I. Fischer, J. García-Ojalvo, C. R. Mirasso, L. Pesquera, and K. A. Shore, Nature (London) **438**, 343 (2005).
[13] K. Yoshimura, J. Muramatsu, P. Davis, T. Harayama, H. Okumura, S. Morikatsu, H. Aida, and A. Uchida, Phys. Rev. Lett. **108**, 070602 (2012).
[14] H. Koizumi, S. Morikatsu, H. Aida, T. Nozawa, I. Kakesu, A. Uchida, K. Yoshimura, J. Muramatsu, and P. Davis, Opt. Express **21**, 17869 (2013).
[15] E. Klein, N. Gross, E. Kopelowitz, M. Rosenbluh, L. Khaykovich, W. Kinzel, and I. Kanter, Phys. Rev. E **74**, 046201 (2006).
[16] M. Peil, T. Heil, I. Fischer, and W. Elsäßer, Phys. Rev. Lett. **88**, 174101 (2002).
[17] T. Heil, I. Fischer, W. Elsässer, J. Mulet, and C. R. Mirasso, Phys. Rev. Lett. **86**, 795 (2001).
[18] J. M. Buldú, T. Heil, I. Fischer, M. C. Torrent, and J. García-Ojalvo, Phys. Rev. Lett. **96**, 024102 (2006).
[19] F. Rogister and J. García-Ojalvo, Opt. Lett. **28**, 1176 (2003).
[20] V. Flunkert, O. D'Huys, J. Danckaert, I. Fischer, and E. Schöll, Phys. Rev. E **79**, 065201 (2009).
[21] E. M. Shahverdiev, S. Sivaprakasam, and K. A. Shore, Phys. Rev. E **66**, 037202 (2002).
[22] E. Shahverdiev, S. Sivaprakasam, and K. Shore, Phys. Lett. A **292**, 320 (2002).
[23] C. Li, X. Liao, and K. Wong, Phys. D **194**, 187 (2004).
[24] J. Mulet, C. Mirasso, T. Heil, and I. Fischer, J. Opt. B: Quantum Semiclassical Opt. **6**, 97 (2004).
[25] C. M. Gonzalez, M. C. Torrent, and J. Garcìa-Ojalvo, Chaos **17**, 033122 (2007).
[26] N. Jiang, W. Pan, B. Luo, L. Yan, S. Xiang, L. Yang, D. Zheng, and N. Li, Phys. Rev. E **81**, 066217 (2010).
[27] T. Deng, G.-Q. Xia, Z.-M. Wu, X.-D. Lin, and J.-G. Wu, Opt. Express **19**, 8762 (2011).
[28] M. Ozaki, H. Someya, T. Mihara, A. Uchida, S. Yoshimori, K. Panajotov, and M. Sciamanna, Phys. Rev. E **79**, 026210 (2009).
[29] T. Sano, Phys. Rev. A **50**, 2719 (1994).
[30] I. Fischer, G. H. M. van Tartwijk, A. M. Levine, W. Elsässer, E. Göbel, and D. Lenstra, Phys. Rev. Lett. **76**, 220 (1996).
[31] W. Ray, W.-S. Lam, P. N. Guzdar, and R. Roy, Phys. Rev. E **73**, 026219 (2006).
[32] D. Brunner, X. Porte, M. C. Soriano, and I. Fischer, Sci. Rep. **2**, 732 (2012).
[33] A. Campos-Mejìa, A. N. Pisarchik, and D. A. Arroyo-Almanza, Chaos, Solitons Fractals **54**, 96 (2013).
[34] K. Kaneko and I. Tsuda, Chaos **13**, 926 (2003).
[35] F. T. Arecchi, G. Giacomelli, P. L. Ramazza, and S. Residori, Phys. Rev. Lett. **65**, 2531 (1990).
[36] K. Otsuka, Phys. Rev. Lett. **65**, 329 (1990).
[37] Y. Miyasaka, K. Otsuka, T. Maniwa, and J.-Y. Ko, Phys. Rev. E **70**, 046208 (2004).
[38] J. Namikawa, Phys. Rev. E **72**, 026204 (2005).

[39] G. Tanaka, M. A. F. Sanjuán, and K. Aihara, Phys. Rev. E **71**, 016219 (2005).
[40] I. Tsuda, H. Fuji, S. Tadokoro, T. Yasuoka, and Y. Yamaguti, J. Integr. Neurosci. **03**, 159 (2004).
[41] H. Nozawa, Phys. D **75**, 179 (1994).
[42] I. Tsuda, Behav. Brain Sci. **24**, 793 (2001).
[43] M. C. Soriano, J. García-Ojalvo, C. R. Mirasso, and I. Fischer, Rev. Mod. Phys. **85**, 421 (2013).
[44] A. Hohl, A. Gavrielides, T. Erneux, and V. Kovanis, Phys. Rev. Lett. **78**, 4745 (1997).
[45] R. Lang and K. Kobayashi, IEEE J. Quantum Electron. **16**, 347 (1980).
[46] B. A. Shenoi, *Introduction to Digital Signal Processing and Filter Design* (John Wiley & Sons, Inc., New York, 2005), Chap. 5, pp. 249–302.
[47] N. Shibasaki, A. Uchida, S. Yoshimori, and P. Davis, IEEE J. Quantum Electron. **42**, 342 (2006).
[48] T. Heil, I. Fischer, and W. Elsäßer, Phys. Rev. A **58**, R2672 (1998).
[49] K. Hicke, O. D'Huys, V. Flunkert, E. Schöll, J. Danckaert, and I. Fischer, Phys. Rev. E **83**, 056211 (2011).
[50] A. Bogatov, P. Eliseev, and B. Sverdlov, IEEE J. Quantum Electron. **11**, 510 (1975).